The Detection of Resonance Frequency in Motion Control Systems

Sheng-Ming Yang, *Member, IEEE*, and Shih-Chuan Wang

***Abstract*—Because of the flexibility of mechanical linkages and high control gains, mechanical resonance may occur, causing torsional vibrations between the motor and load in servo control systems. These vibrations generate velocity and positioning errors for the control system and may damage the system components. This study presents a resonance frequency tracking scheme for servo control systems. The scheme uses velocity error and bandpass filters to track resonance frequencies. After detection, a notch filter in series to the current command is enabled to suppress the vibration. This scheme can be employed during the initial setup and for online resonance frequency tracking. In addition, the proposed scheme can be used to identify all vibrational frequencies in systems with multiple resonant frequencies.**

***Index Terms*—Frequency tracking, motion control, resonance.**

I. Introduction

SERVO control systems are used in a wide range of industrial applications such as automated machines, robotics, and machine tools. Most of these systems are composed of gears, belts, and couplings. Because of the flexibility of these mechanical components and high control gains, mechanical resonance may occur, causing torsional vibrations between the motor and load in servo control systems. The continued vibration of mechanical linkages can damage these components and generate positioning errors in the motor drive. Therefore, the detection and suppression of torsional vibrations are critical to the operation of servo motor drives.

Many techniques for overcoming mechanical resonance have been proposed. Torsional vibrations can be reduced using measurements of load velocity and acceleration feedback [1], [2]. Certain schemes use fast Fourier transform [3]–[6], shifted discrete Fourier translations [7], or discrete wavelet transforms [8] to calculate the resonance frequency before tuning filters to suppress resonance vibrations. The implementation of these schemes generally necessitates complex theories, calculations, and powerful memory. Alternative strategies for estimating resonance frequency are presented in [9], whereby frequency weighting functions are used to scan the system. However, the algorithm is complex and difficult to implement for industrial servo drives. Disturbance observers are also employed to feedback torsion torque and vibration suppressions [10]–[15]. These techniques also require prior knowledge of drive parameters such as torque constant for implementation.

In this paper, a novel resonance frequency detection scheme for servo control systems is presented. The scheme uses velocity errors and bandpass filters to track resonance frequencies. After detection, a notch filter in series to the current command is enabled to suppress the vibrations.

Manuscript received October 21, 2013; revised January 22, 2014; accepted February 3, 2014. Date of publication February 20, 2014; date of current version September 16, 2014. Paper 2013-IDC-831.R1, presented at the 2013 IEEE Energy Conversion Congress and Exposition, Denver, CO, USA, September 16–20, and approved for publication in the IEEE TRANSACTIONS ON INDUSTRY APPLICATIONS by the Industrial Drives Committee of the IEEE industry Applications Society. This work was supported by the National Science Council, Taiwan, under Grant NSC 99-2221-E-027-113-MY3.

The authors are with the Department of Electrical Engineering, National Taipei University of Technology, Taipei 10608, Taiwan (e-mail: smyang@ntut.edu.tw; edison_0915@yahoo.com.tw).

Color versions of one or more of the figures in this paper are available online at http://ieeexplore.ieee.org.

Digital Object Identifier 10.1109/TIA.2014.2306982

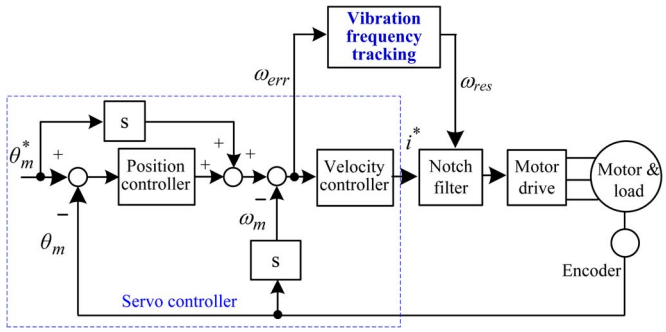

Fig. 1. Block diagram of the servo control and the vibration frequency tracking system.

II. System Model and Signal Preprocessor

Fig. 1 shows a block diagram of a servo control system with the proposed resonance frequency tracking and suppression system. The motor controller has a cascaded position and velocity control loop. Motor position and velocity errors are regulated separately in these loops. When the motor with resonant load is operated, vibrations occur in controller errors and the drive current command (i^*). The proposed scheme uses velocity errors as a source for detecting vibration frequency, although position errors and the drive current can also be employed. In addition, the scheme can be applied to other types of position- and velocity-controlled systems. As shown in Fig. 1, the calculated vibration frequency is loaded into a notch filter in series with the current command to suppress vibrations.

At the beginning of the resonance frequency tracking process, a segment of velocity errors are sampled and stored, and data are denoted as $\omega_{err}(t)$. The sampling process is established to facilitate the acquisition of at least one error vibration cycle. Preprocessing is then performed with these data. Fig. 2 is a flowchart of the preprocessing procedure. First, a high-pass filter is used to remove the low frequency and dc components in velocity errors. A bandpass filter is then applied to discriminate

Fig. 2. Flowchart for the preprocessor.

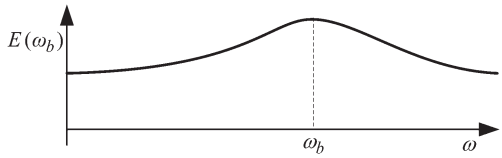

Fig. 3. Typical frequency response of the preprocessor output.

the frequency content of the errors. The transfer function of the bandpass filter can be expressed as

$$\frac{\omega_{errf}}{\omega_{err}} = \frac{2\zeta\omega_b s}{s^2 + 2\zeta\omega_b s + \omega_b^2} \tag{1}$$

where ζ is a constant, ω_b represents the frequency of the bandpass filter, and ω_{errf} represents the filtered output. Finally, the average absolute value of the filtered outputs is calculated. The preprocessor can be expressed as follows:

$$E(\omega_b) = \frac{1}{T}\int_0^T |BPF\left[HPF\left(\omega_{err}(t)\right)\right]|\, dt \tag{2}$$

where $E(\omega_b)$ represents the preprocessor output and BPF and HPF represent the bandpass and high-pass filtering, respectively. Fig. 3 shows a typical preprocessor frequency response when the velocity error contains only one vibrational frequency component. According to the figure, the maximum $E(\omega_b)$ occurs at $\omega = \omega_b$. This property is used to track resonance frequency.

III. Resonance Frequency Tracking

The proposed resonance frequency tracking scheme can be performed when the motor is operating at constant speed or at a standstill. Fig. 4 shows the flowchart of the tracking process. Before the process begins, a segment of velocity error is sampled and stored. The preprocessing described in the preceding section is then performed for three bandpass filter frequencies: ω_b, $\omega_b - \Delta\omega$, and $\omega_b - 2\Delta\omega$, where $\Delta\omega$ is an incremental frequency. The initial ω_b can be set to a known resonance frequency in the start-up of the motor drive or simply set to one of the boundaries of the region in which resonance is likely to occur. For the convenience of explanation, $\Delta\omega$ is set to 1 Hz. Therefore, the frequencies calculated with the preprocessor become ω_b, $\omega_b - 1$, and $\omega_b - 2$ Hz, and their outputs are denoted as $E(\omega_b)$, $E(\omega_b - 1)$, and $E(\omega_b - 2)$, respectively. After the preprocessing, the slope between $E(\omega_b)$ and $E(\omega_b - 1)$ is calculated and denoted as S.

Three possible modes for the preprocessor outputs exist. As shown in Fig. 5, the first mode is that all the outputs are located to the left of the resonance frequency, the second mode is that all outputs are located to the right of the resonance frequency, and the third mode is that the resonance frequency is located between ω_b and $\omega_b - 2$. Note that arrangements

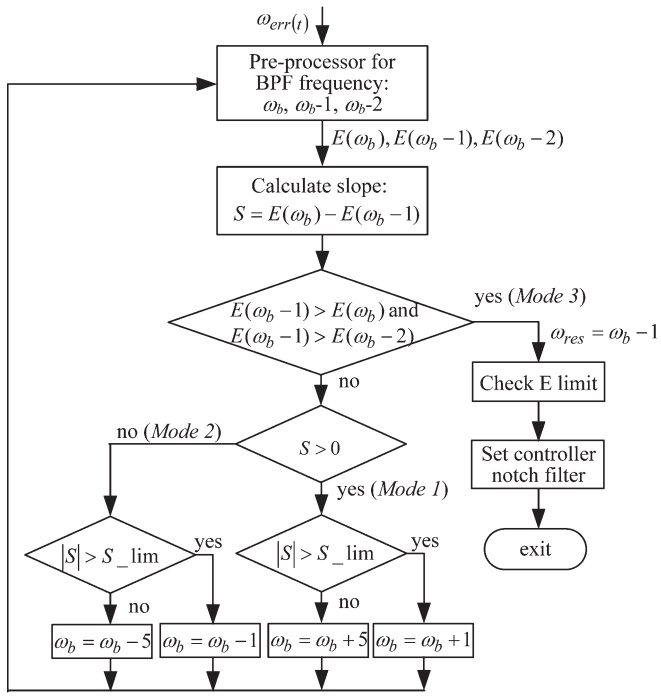

Fig. 4. Flowchart of the frequency tracking process.

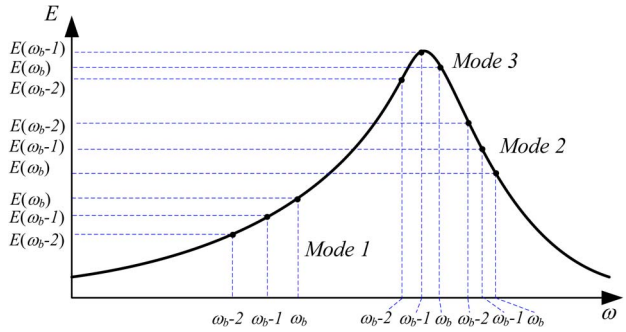

Fig. 5. Modes of the preprocessor outputs.

aside from those mentioned previously were ignored because they were caused by either a small vibrational frequency or measurement errors. Accordingly, the mode of the processed frequencies can be determined easily by comparing the three preprocessor outputs. If the results indicate the third mode, i.e., $E(\omega_b - 1)$ is located between $E(\omega_b)$ and $E(\omega_b - 2)$, the process is stopped, and $\omega_b - 1$ is the resonance frequency. This frequency is denoted as ω_{res} in the flowchart of Fig. 4.

In the cases of Modes 1 and 2, the iteration of ω_b is required to track the resonance frequency. The polarity of slope S is examined to determinate these modes. Positive S suggests that the current ω_b is smaller than the actual resonance frequency and ω_b should be increased in the following iteration. By contrast, negative S suggests that the current ω_b exceeds the actual resonance frequency and ω_b should be reduced in the following iteration. Note that this algorithm is a variation of the maximum power point tracking scheme generally used for photovoltaic systems [16]. The incremental frequency can be set to a fixed value for simplicity. However, to reduce the tracking time, incremental frequency is set to a low value (e.g., 1 Hz) if the slope is higher than a preset limit (S_lim); otherwise, it is set

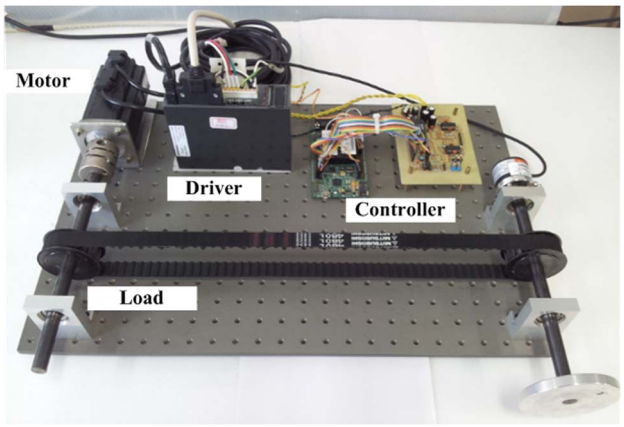

Fig. 6. Experimental System A.

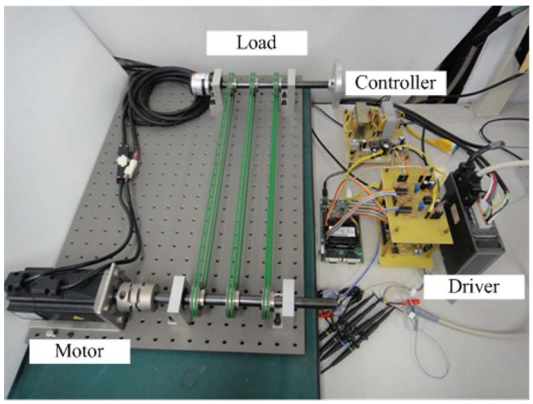

Fig. 7. Experimental System B.

to a higher value (e.g., 5 Hz). After the new ω_b is determined, the prestored data are reprocessed.

After tracking is completed, $E(\omega_{res})$ is checked to determine whether the amplitude of the oscillation is sufficient to initiate the controller notch filter. The E limit can be adjusted according to the allowable maximum velocity ripple of the motor drive; in this study, it was set to approximately $+-10$ r/min oscillations of the velocity error. The controller notch filter was set to ω_{res} if $E(\omega_{res})$ exceeded this value; otherwise, it was disabled.

The proposed scheme can be employed for the initial setup as well as online resonance frequency tracking. Furthermore, by implementing minor modifications, the proposed scheme can also be used to identify all vibration frequencies in systems with multiple resonance frequencies. In these systems, $E(\omega)$ versus ω plots have multiple peaks. These peaks can be identified, and their associated controller notch filters can be set sequentially. However, the tracking process becomes more complicated since each resonance requires a process shown in Fig. 4 to track its frequency.

IV. Experiment Results

A 400-W 1200-r/min permanent-magnet synchronous servo motor drive was used for experimental verification. Two mechanical loads were established for the motor drive, as shown in Figs. 6 and 7. Both systems contained pulleys, belts, linkages, and an inertia disk. Because the stiffness of the belts used in these systems differed, the resonance frequencies of Systems A and B were approximately 380 and 30 Hz, respectively. In both systems, an encoder was attached to the rotary shaft with a load disk for performance evaluations. A digital signal processor was used to control the motor and detect and track the resonance frequency. The controller was executed at 5 kHz. The controller gains were tuned to ensure controller stability when the belts and load disk were disconnected. Velocity errors of approximately 0.1 s in length were sampled for the preprocessor.

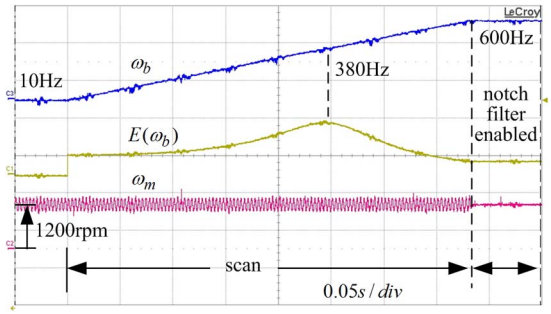

Fig. 8. Experimental System A was scanned from 10 to 600 Hz, controller notch filter was set to 380 Hz after the scan completed, and motor was operated at 1200 r/min.

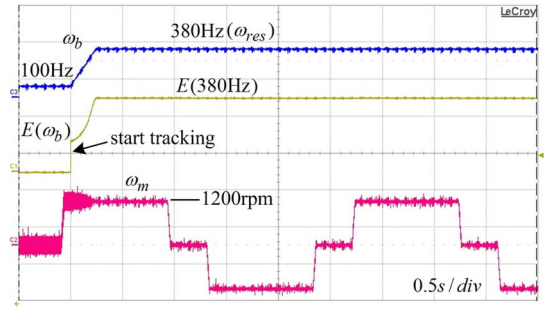

Fig. 9. Resonance frequency tracking response for System A when $\omega_m = 1200$ r/min and initial frequency was set to $\omega_b = 100$ Hz.

A. Experimental Results for System A

Fig. 8 shows the results of resonance frequency scanning when the motor was operated at 1200 r/min. In this experiment, the preprocessing technique shown in Fig. 4 was performed with ω_b varying from 10 to 600 Hz. The frequency of maximum E was calculated during the scanning process. The controller notch filter was set to this frequency immediately after the scan was complete. The results in Fig. 8 show that the maximum E occurs at approximately 380 Hz, which is the system resonance frequency. Regarding motor speed, considerable oscillations were observed during scanning; however, these oscillations ceased after the controller notch filter was set.

Figs. 9 and 10 show the resonance frequency tracking response when the motor was operated at 1200 r/min; the initial frequency was set to 100 and 600 Hz, respectively. Fig. 11 shows an amplified view of the region where the tracking was performed in Fig. 9. The results show that, for both cases, tracking was completed in less than 0.3 s. In this experiment, the frequency of the controller notch filter was set to ω_b after each iteration to examine the effectiveness of the tracking algorithm.

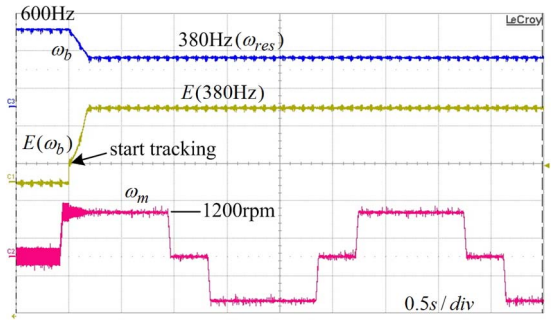

Fig. 10. Resonance frequency tracking response for System A when $\omega_m = 1200$ r/min and initial frequency was set to $\omega_b = 600$ Hz.

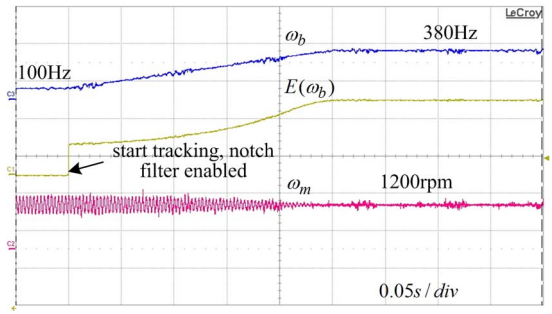

Fig. 11. Amplified view of the region just after the tracking started in Fig. 9.

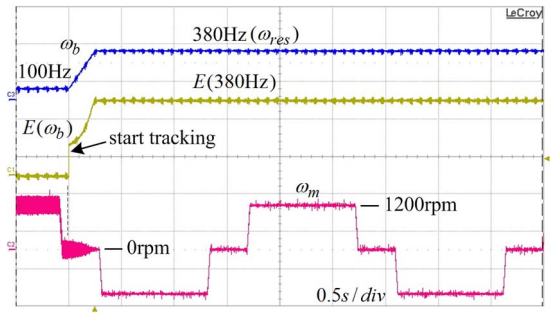

Fig. 12. Resonance frequency tracking response for System A when $\omega_m = 0$ r/min and initial tracking frequency $\omega_b = 100$ Hz.

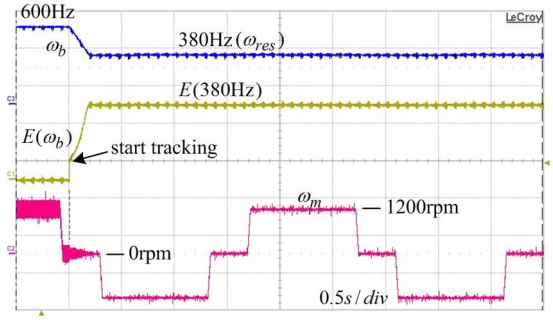

Fig. 13. Resonance frequency tracking response for System A when $\omega_m = 0$ r/min and initial tracking frequency $\omega_b = 600$ Hz.

Consequently, the velocity oscillations declined gradually as ω_b approached the resonance frequency.

Figs. 12 and 13 show the resonance frequency tracking response when the motor was at standstill; the initial frequency was set to 100 and 600 Hz, respectively. The results are similar to those shown in Figs. 9 and 10. The tracking process converged to the correct resonance frequency within 0.3 s. In addition, based on experimental results not presented in this paper, the tracking process can be executed at any speeds within the range of the motor drive, and the time required for convergence is generally less than 0.3 s. Furthermore, the execution time can be reduced by reducing the length of the data processed.

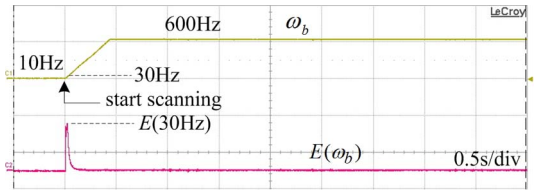

Fig. 14. Experimental System B was scanned from 10 to 600 Hz, and motor was operated at 1200 r/min.

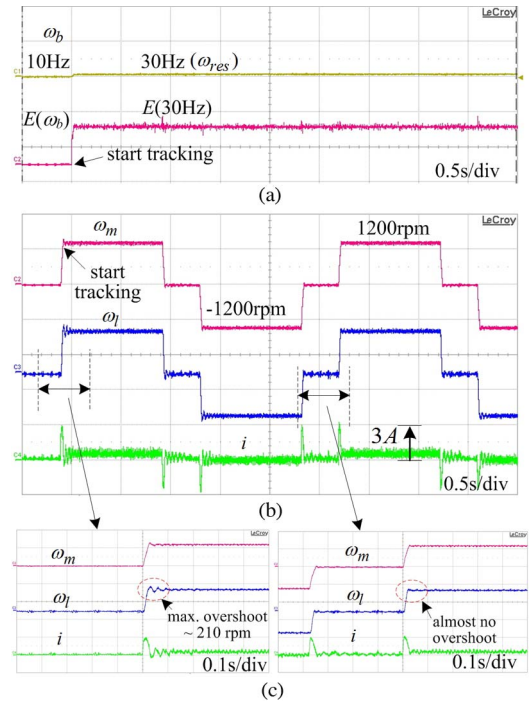

Fig. 15. Resonance frequency tracking response for System B when $\omega_m = 1200$ r/min and initial frequency was set to $\omega_b = 10$ Hz. (a) ω_b and $E(\omega_b)$. (b) Motor, load speed, and current. (c) Amplified views.

B. Experimental Results for System B

Fig. 14 shows the results of the resonance frequency scanning of Experimental System B when the motor was operated at 1200 r/min. In this experiment, the preprocessing technique shown in Fig. 2 was performed with ω_b varying from 10 to 600 Hz. The results show that the maximum E occurs at approximately 30 Hz, which is the System B resonance frequency.

Fig. 15 shows the results of the vibration frequency tracking when the motor was operated at 1200 r/min. The initial ω_b was set to 10 Hz. In addition, ω_l represented the speed of the load

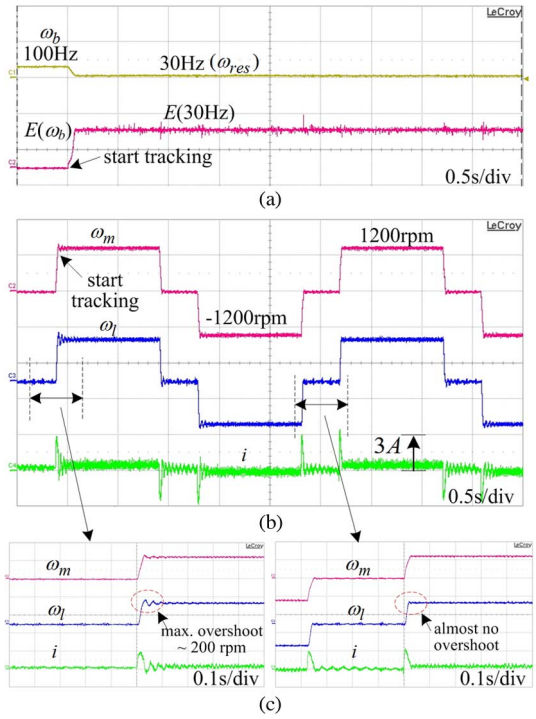

Fig. 16. Resonance frequency tracking response for System B when $\omega_m = 1200$ r/min and initial frequency was set to $\omega_b = 100$ Hz. (a) ω_b and $E(\omega_b)$. (b) Motor, load speed, and current. (c) Amplified views.

disk. The frequency of the controller notch filter was set to the tracked frequency immediately after each iteration. Fig. 15(c) shows an amplified view of the region in Fig. 15(b) where tracking was performed. According to Fig. 15(b) and (c), the motor and load speed responses exhibited substantial oscillations when tracking was initiated, and maximum overshoot was about 210 r/min. However, the oscillations diminished after the controller notch filter was set to the appropriate frequency, and tracking was completed in less than 0.1 s.

Fig. 16 shows the same waveforms as those presented in Fig. 15, except that the initial frequency was set to 100 Hz for resonance frequency tracking. Similarly, ω_b converged to 30 Hz shortly after tracking began. Notably, tracking conducted when the motor is at a standstill can yield similar results.

V. Conclusion

This study presented a resonance frequency detection and suppression scheme for servo control systems. The proposed scheme uses velocity errors and bandpass filters to track vibration frequencies. After detection, a notch filter in series with the current command is set to suppress motor vibrations. The proposed scheme was verified experimentally. The results showed that the proposed scheme can effectively detect and suppress resonance vibrations ranging between 30 and 380 Hz. Furthermore, the operation of the scheme at any speeds within the speed range of the motor drive was stable. The time required for convergence was generally less than 0.3 s, declining further when the initial frequency is near the resonance frequency.

References

[1] S. Vukosavic and M. Stojic, "Suppression of torsional oscillations in a high-performance speed servo drive," *IEEE Trans. Ind. Electron.*, vol. 45, no. 1, pp. 108–117, Feb. 1998.
[2] T. Tang, "Reduction of mechanical resonance based on load acceleration feedback for servo system," *Electron. Eng.*, vol. 34, no. 7, pp. 15–17, 2007.
[3] P. Schmidt and T. Rehm, "Notch filter tuning for resonant frequency reduction in dual inertia systems," in *Conf. Rec. IEEE IAS Annu. Meeting*, Oct. 1999, pp. 1730–1734.
[4] T. Rehm and P. Schmidt, "Method and apparatus for reducing resonance in a dual inertia system," U.S. Patent 6 144 181, Nov. 7, 2000.
[5] H. Wang, "Vibration rejection scheme of servo drive system with adaptive notch filter," in *Proc. 37th IEEE PESC*, 2006, pp. 1–6.
[6] D.-H. Lee, J. H. Lee, and J.-W. Ahn, "Mechanical vibration reduction control of two-mass permanent magnet synchronous motor using adaptive notch filter with fast Fourier transform analysis," *IET Elect. Power Appl.*, vol. 6, no. 7, pp. 455–461, Aug. 2012.
[7] J. Kang, S. Chen, and X. Di, "Online detection and suppression of mechanical resonance for servo system," in *Proc. ICICIP*, Jul. 2012, pp. 16–21.
[8] S. H. Kia, H. Henao, and G.-A. Capolino, "Torsional vibration assessment using induction machine electromagnetic torque estimation," *IEEE Trans. Ind. Electron.*, vol. 57, no. 1, pp. 209–219, Jan. 2010.
[9] K. Ohno and T. Hara, "Adaptive resonant mode compensation for hard disk drives," *IEEE Trans. Ind. Electron.*, vol. 5, no. 2, pp. 624–630, Apr. 2006.
[10] H. Kawaharada, I. Godler, T. Ninomiya, and H. Honda, "Vibration suppression control in 2-inertia system by using estimated torsion torque," in *Proc. IEEE IECON*, Oct. 2000, pp. 2219–2224.
[11] K. Sugiura and Y. Hori, "Vibration suppression in 2- and 3-mass system based on the feedback of imperfect derivative of the estimated torsional torque," *IEEE Trans. Ind. Electron.*, vol. 43, no. 1, pp. 56–64, Feb. 1996.
[12] H. Nakamura and K. Kaisha, "Mechanical vibration detector and vibration damping controller," U.S. Patent 5 990 645, Nov. 23, 1999.
[13] L. Huang, D. Qu, and F. Xu, "Adjustable inertia ratio control for low-frequency torsional resonance suppression in industrial servo system," in *Proc. ICMTMA*, Mar. 2010, pp. 432–435.
[14] S. Katsura and K. Ohnishi, "Force servoing by flexible manipulator based on resonance ratio control," *IEEE Trans. Ind. Electron.*, vol. 54, no. 1, pp. 539–547, Feb. 2007.
[15] M. A. Valenzuela, J. M. Bentley, A. Villablanca, and R. D. Lorenz, "Dynamic compensation of torsional oscillation in paper machine sections," *IEEE Trans. Ind. Appl.*, vol. 41, no. 6, pp. 1458–1466, Nov./Dec. 2005.
[16] W. Xiao, A. Elnosh, V. Khadkikar, and H. Zeineldin, "Overview of maximum power point tracking technologies for photovoltaic power systems," in *Proc. IEEE IECON*, Nov. 2011, pp. 3900–3905.

Sheng-Ming Yang (S'87–M'90) received the M.S. and Ph.D. degrees from the University of Wisconsin–Madison, Madison, WI, USA, in 1985 and 1989, respectively.

From 1989 to 1992, he was a Development Engineer with Unico Inc., Franksville, WI, USA, and from 1992 to 1995, he was a Principal Engineer at the Corporate Technology Center, A. O. Smith Company, Milwaukee, WI, USA. In 1995, he has been with Tamkang University, Taipei, Taiwan, as a Professor in the Department of Mechanical and Electro-Mechanical Engineering. Since 2007, he has been with the Department of Electrical Engineering, National Taipei University of Technology, Taipei. His research interests are ac and dc motor drives and control.

Shih-Chuan Wang was born in Taipei, Taiwan, on September 15, 1987. He received the M.S. degree in electrical engineering from the National Taipei University of Technology, Taipei, in 2013.

His research interests are ac motor drives and control.